

Grid-Tied Pv System With Fuzzy Based Single-Phase Transformerless Inverter With Charge Pump Circuit Concept

P.Vasavi Reddy & Md. Jani Pasha

¹M.Tech, B V Raju Institute of technology, Narsapur, Hyderabad, Telangana.

²Assistant Professor, B V Raju Institute of technology, Narsapur, Hyderabad, Telangana.

ABSTRACT: In this paper we are implementing a single phase transformer less photovoltaic inverter for grid connect PV system. In this topology we are developing the concept of a charge pump circuit in order to eliminate the leakage current. We are utilizing the fuzzy controller in this paper. We are comparing the fuzzy controller with other controller. The neutral of the grid is directly connected to the negative polarity of the PV panel that creates a constant common mode voltage and zero leakage current. During the negative cycle, the charge pump circuit generates the negative output voltage of the proposed inverter. Therefore according to the proportional resonant control strategy is used to control the injected current. There are various advantage of the proposed inverter they are the neutral of the grid is directly connected to the negative terminal of the PV panel, so the leakage current is eliminated, its compact size; low cost; the used dc voltage of the proposed inverter is the same as the full-bridge inverter (unlike neutral point clamped (NPC), active NPC, and half-bridge inverters); flexible grounding configuration; capability of reactive power flow; and high efficiency. By using simulation result we can verify the concept of the proposed inverter and its practical application in grid-tied PV systems.

Index Terms—Charge pump circuit, grid-tied inverter, leakage current elimination, transformer less inverter, fuzzy control.

INTRODUCTION

From the recent year we are developing the photovoltaic (PV) power systems have become very popular among the renewable energy sources, because they generate electricity with no moving parts, operate quietly with no emissions, and require little maintenance [1], [2]. Distributed grid-connected PVs are playing an increasingly role as an integral part of the electrical grid. However, due to the large stray capacitors between the PV panels and the ground, PV systems suffer from a high common mode (CM) current, which reduces the system efficiency and may cause safety issues like electric shock.

In order to eliminate the leakage currents, transformers are commonly used in the PV system to provide galvanic isolation. One of the important issues in the transformerless gridconnected PV applications is the galvanic connection of the grid and PV system, which leads to leakage current problems. For transformerless grid-connected inverters, full-bridge (FB) inverter, neutral point clamped (NPC), active NPC (ANPC) inverter [5], and many other topologies such as H5, H6, and highly efficient

and reliable inverter concept (HERIC) were proposed to reduce the leakage current with disconnecting of the grid from the PV during the freewheeling modes [6]. Fig. 1 illustrates a single-phase grid-tied transformerless inverter with CM current path, where P and N are the positive and negative terminals of the PV, respectively. The leakage current ($i_{Leakage}$) flows through a parasitic capacitor (C_p) between the filters (L_1 and L_2), the inverter, grid, and ground impedance (z_g). This leakage current may cause safety problems, reduce the quality of injection current to the grid, as well as decrease the system efficiency [8]. In order to eliminate the leakage current, the CM voltage (CMV) (v_{cm})

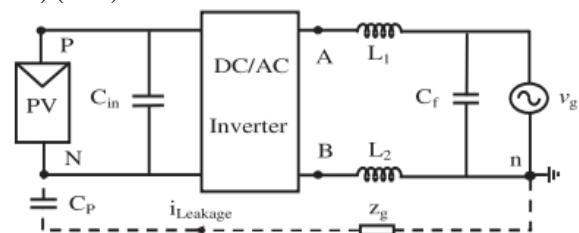


Fig. 1. Block diagram of a single-phase grid-connected transformer less inverter with a leakage current path.

must be kept constant during all operation modes according to [9]. The v_{cm} with two filter inductors (L_1, L_2) is calculated as follows:

$$v_{cm} = \frac{v_{An} + v_{Bn}}{2} + \frac{(v_{An} - v_{Bn})(L_1 - L_2)}{2(L_1 + L_2)} \quad (1)$$

where v_{An} and v_{Bn} are the voltage differences between the midpoints A and B of the inverter to the dc bus minus terminal N, respectively. If $L_1 = L_2$ (asymmetrical inductor), v_{cm} is calculated according to (1) and the leakage current appears due to a varying CMV. If $L_1 \neq L_2$ (symmetrical inductor), v_{cm} is simplified to

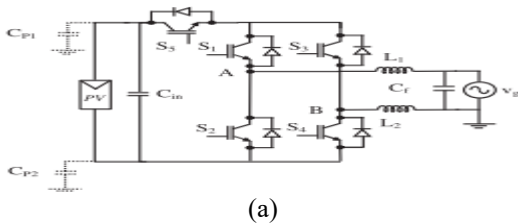
$$v_{cm} = \frac{v_{An} + v_{Bn}}{2} = \text{Cons} \quad (2)$$

In this state, the CMV is constant and the leakage current is eliminated. In some structures such as the virtual dc-bus inverter [10] and NPC inverter, one of the filter inductors is zero and only one filter inductor is used. In this state, after simplification of v_{cm} , it will have a constant value according to (3) and the leakage current will be eliminated

$$v_{cm} = \frac{v_{An} + v_{Bn}}{2} + \frac{v_{An} - v_{Bn}}{2} = \text{Const.} (L_1 = 0) \quad v_{cm} = \frac{v_{An} + v_{Bn}}{2} - \frac{v_{An} - v_{Bn}}{2} = \text{Const.} (L_1 = 0) \quad (3)$$

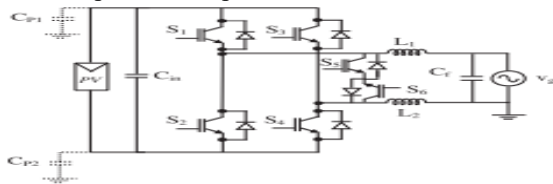
As shown in Fig. 2, there are various transformerless grid connected inverters based on the FB inverter in the literature to overcome these problems.

The H5 inverter that is a FB-based inverter topology, compared to the conventional FB inverter, needs one additional switch (S5) on the dc side to decouple the dc side from the grid as shown in Fig. 2(a).



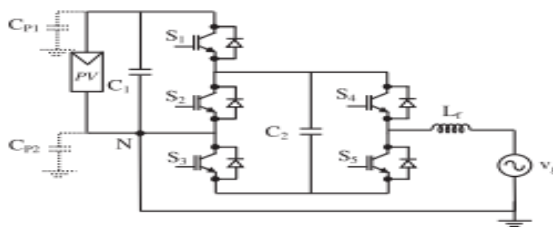
(a)

As shown in Fig. 2(b), the HERIC topology needs two extra switches on the ac side to decouple the ac side from the PV module in the zero stage. HERIC combines the merits of unipolar and bipolar modulation.



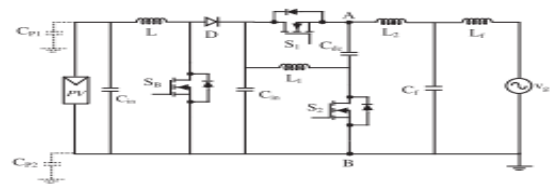
(b)

Another solution to eliminate the leakage current is the direct connection of the negative PV terminal to the neutral point of the grid, such as the virtual dc-bus inverter and the unusual topology. As shown in Fig. 2(c), the virtual dc-bus inverter is composed of five insulated-gate bipolar transistors (IGBTs), two capacitors, and one filter inductor Lf.



(c)

The virtual dc-bus generates the negative output voltage. The main drawback of this topology is that there is no path to charge the capacitor C2 during the negative cycle and this will cause a high output total harmonic distortion (THD). The topology presented, which is shown in Fig. 2(d), has a common ground with the grid.



(d)

Fig. 2. Single-phase grid-tied transformerless PV inverter topologies: (a) H5 inverter, (b) HERIC inverter, (c) virtual dc-bus inverter [10], and (d) CM inverter proposed

The number of semiconductors used in this topology is low. However, the output voltage of this inverter is only two levels including positive and negative voltages without creating the zero voltage, which requires a large output inductor L2 and a filter. The inductor medium-type inverter also called “Karschny” is another topology that is derived from the buck–boost topology.

This paper introduces a new transformerless inverter based on charge pump circuit concept, which eliminates the leakage current of the grid-connected PV systems using a unipolar sinusoidal pulse width modulation (SPWM) technique. The proposed topology consists of only four power switches, so the cost of the semiconductors is reduced and the power quality is improved by three-level output voltage in order to reduce the output current ripple.

PROPOSED TOPOLOGY AND MODULATION STRATEGY

A.Charge Pump Circuit Concept

The concept of a simple charge pump circuit to be used in the proposed topology to generate the inverter negative output voltage is shown in Fig. 3. The circuit consists of two diodes (D1, D2) and two capacitors (C1, C2). The capacitor C1 is used to couple the voltage point of A to the node D. Two Schottky diodes D1 and D2 are used to pump the output voltage.

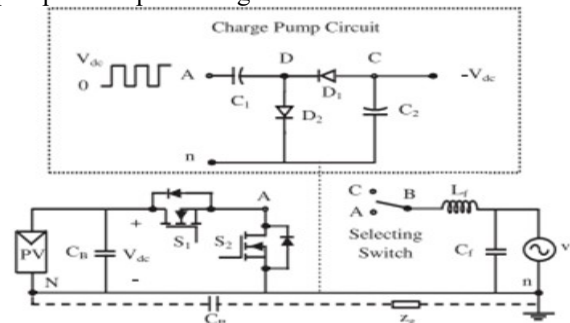


Fig. 3. Schematic diagram of the proposed inverter including the charge pump circuit.

In steady state, the output voltage of the negative charge pump circuit (v_{Cn}) can be derived by

$$v_{Cn} = -V_{dc} + V_{cut-in-D1} + V_{cut-in-D2} \quad (4)$$

where V_{dc} is the input voltage, $V_{cut-in-D1}$ and $V_{cut-in-D2}$ are the cut-in voltages of the diodes D1 and

D2, respectively. For high power applications, these values can be negligible.

The above principle is integrated into the proposed inverter by using additional switching devices. In summary, the charge pump circuit in the transformerless inverter has the following characteristics for grid-tied applications.

1) This circuit has a common line with the negative terminal of the input dc voltage and the neutral point of the grid that causes the leakage current to be eliminated.

2) The charge pump circuit has no active device and it has a lower cost for grid-tied applications.

B. Proposed Topology

As shown in Fig. 4, the proposed topology consists of four power switches ($S_1 - S_4$), two diodes (D_1, D_2), two capacitors (C_1, C_2) based on the charge pump circuit as described in Section II-A.

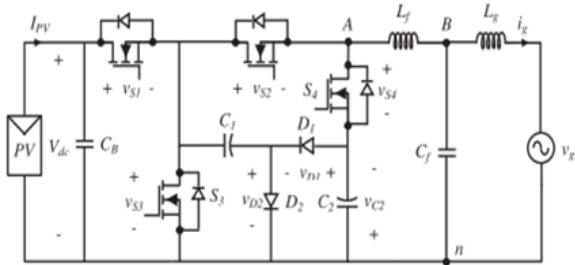


Fig. 4. Proposed single-phase transformerless grid-connected inverter

This new topology is modulated using simple SPWM. Fig. 5 shows the gate drive signals for the proposed inverter under the current lagging condition. According to the direction of the inverter output voltage and output current, the operation of the proposed inverter is divided in four regions as shown in Fig. 6.

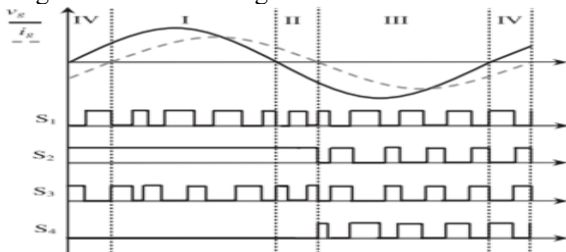
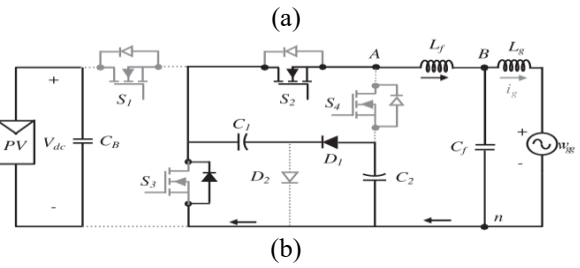
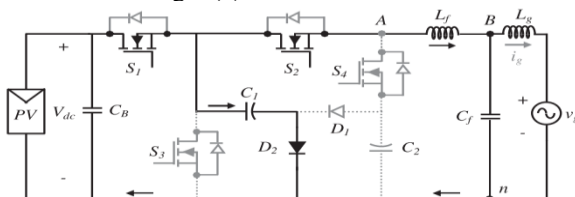
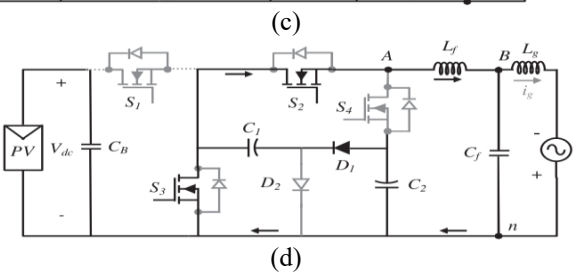
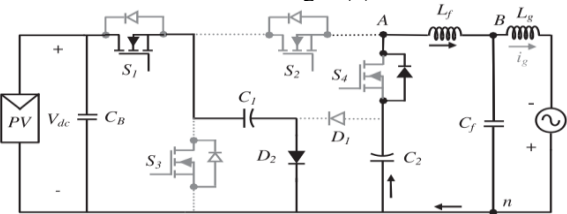


Fig. 5. Switching pattern of the proposed topology with reactive power flow.

Region I: the inverter output voltage and the output current are positive; energy is transferred from dc side to grid side as shown in Fig. 6(a).

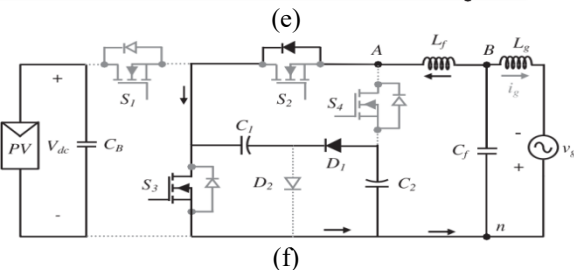
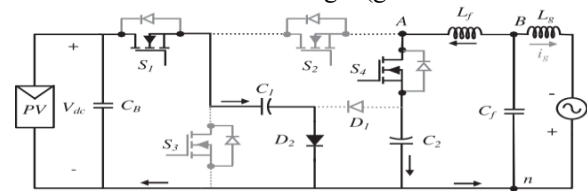


Region II: the inverter output voltage is negative and the output current is positive; energy is transferred from grid side to dc link as shown in Fig. 6(c).



Region III: the inverter output voltage and the output current are negative; energy is transferred from dc link to grid side as shown in Fig. 6(e).

Region IV: the inverter output voltage is positive and the output current is negative; energy is transferred from grid side to dc link as shown in Fig. 6(g)



When the switches S_1 and S_2 are ON, the output voltage of the inverter (v_{An}) will be $+V_{dc}$ (positive state) as shown in Fig. 6(a) and (g). During this time interval, diode D_1 is reverse biased and D_2 is ON, so the capacitor C_1 is charged through diode D_2 and the voltage across the

capacitor C2 maintains to be constant. In this state, when the switches S2 and S3 are ON, v_{An} will be 0 (zero state) as shown in Fig. 6(b) and (h).

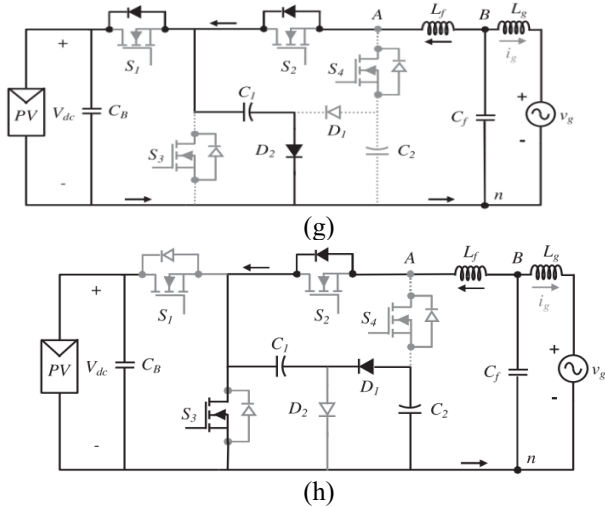


Fig. 6: operational stages of the proposed inverter during (a),(b) region I,(c),(d) region II,(e),(f) Region III and (g),(h) region IV (a) $v_{An} = +V_{dc}, i_g > 0$. (b) $v_{An} = 0, i_g > 0$. (c) $v_{An} = -V_{dc}, i_g > 0$. (d) $v_{An} = 0, i_g > 0$. (e) $v_{An} = -V_{dc}, i_g < 0$. (f) $v_{An} = 0, i_g < 0$. (g) $v_{An} = +V_{dc}, i_g < 0$. (h) $v_{An} = 0, i_g < 0$

In the regions II and III, the negative and zero voltage levels are produced. Fig. 6(c) and (e) shows the equivalent circuit that S4 and S1 are ON. The negative voltage is generated, when switch S4 is turned ON and the voltage across the capacitor C2 appears at the inverter output voltage ($v_{An} = -V_{dc}$) (negative state).

The voltage across the capacitor C1 can be kept constant in this state by the modulation strategy. In this period, the circuit operation of the zero state is similar to the zero state of positive half-period of the grid as shown in Fig. 6(b) and (h). In this case, the charging time constant of capacitor C2 (τ_{C2}) can be expressed as follows:

$$\tau_{C2} = R_{e1}C_{e1} \quad (5)$$

The current through capacitors (iCapacitors) is calculated by

$$i_{Capacitors} = C_{e1} \frac{V_{C1} - V_{C2}}{\tau_{C2}} \quad (6)$$

According to (5), the charging time constant of C2 is larger than its natural discharging time constant and VC1 - VC2 has a very small value in steady state.

ANALYSIS OF THE PROPOSED TOPOLOGY

A. Current Stress Analysis and Capacitors Design

A current stress analysis of the proposed topology is presented in this section. The maximum value of the current stress occur on the switches S1 and S3, because the capacitor C1 is charged through switch S1 and the capacitor C2 is charged through switch S3. Using the PSCAD software, simulation results of the current in the switches

S1 and S3 for an output power of 500 W are shown in Fig. 7.

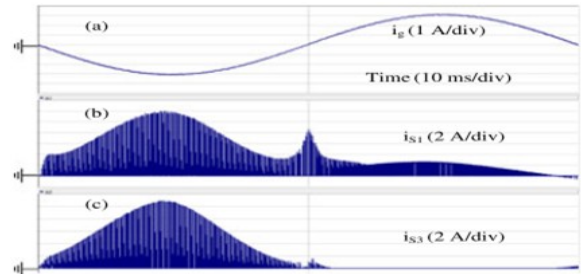


Fig. 7. Simulations of the current of switches: (a) grid current (i_g) [1 A/div], (b) (i_{S1}) [2 A/div], and (c) (i_{S3}) [2 A/div].

The selected parameters of the simulations are the same as the simulation 500 W prototype. These parameters are listed in Table IV. The maximum value of the current in these switches occurs at the negative state in simulation results as shown in Fig. 7. In the negative half-period of the grid, the circuit shifts between the negative and zero states. During the negative state, the capacitor C1 is charged by the capacitor CB, while the capacitor C2 is discharged by the grid.

Therefore, the voltage difference between the capacitors C1 and CB as well as the capacitors C1 and C2 is decreased. The equivalent circuits of the zero and negative states of the proposed topology for the current stress analysis are shown in Fig. 8(a) and (b), respectively.

According to the electric circuit theory, the grid voltage in series with a grid-side inductor (L_g) can be equivalent with the current source (i_g) as shown in Fig. 8.

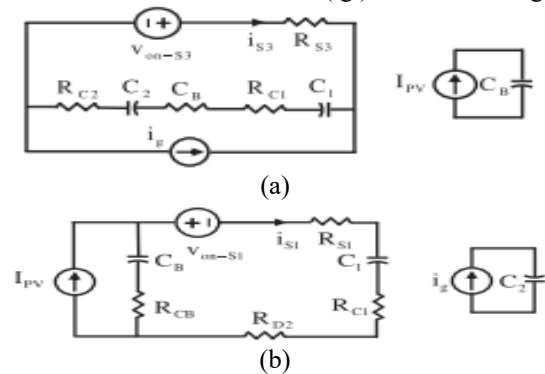


Fig. 8. Equivalent circuit of the proposed converter during (a) zero state and (b) negative state.

According to Fig. 8(a), at the zero state

$$\frac{dv_{diff,1}}{dt} = \frac{v_{diff,1} - R_{S3}i_g}{(R_{e1} + R_{S3})C_{e1}} \quad (7)$$

$$\frac{dv_{diff,2}}{dt} = \frac{I_{PV}}{C_B} - \frac{v_{diff,1} - R_{S3}i_g}{(R_{e1} + R_{S3})C_1} \quad (8)$$

According to Fig. 8(b), in the negative state

$$\frac{dv_{diff,1}}{dt} = \frac{R_{Cb}I_{PV} + v_{diff,2}}{(R_{cb} + R_{e2})C_1} + \frac{i_g}{C_2} \quad (9)$$

$$\frac{dv_{diff,2}}{dt} = \frac{I_{PV}}{C_B} + \frac{R_{CB}I_{PV} - v_{diff,2}}{R_{e2}C_{e2}} \quad (10)$$

where in (8)–(11), R_{e2} and C_{e2} will be as follows:

$$R_{e2} = R_{D2} + R_{S1} + R_{C1} + R_{CB}, C_{e2} = \frac{C_1 C_B}{C_1 + C_B} \quad (11)$$

By using the averaging method at the switching cycle T_s , and linearizing (8)–(11), the average value of $i_S 1$ and $i_S 3$ at the negative and zero states is equal to (13) and (14), respectively:

$$\frac{dv_{diff,1}}{dt} = (1 + s(t)) \frac{v_{diff,1} - R_{S3}i_g}{(R_{e1} + R_{e2})C_{e1}} - s(t) \left(\frac{R_{CB}I_{PV} + v_{diff,2}}{(R_{CB} + R_{e2})C_1} + i_{gC2} \right)$$

$$\frac{dv_{diff,2}}{dt} = (1 + s(t)) \left(\frac{I_{PV}}{C_B} - \frac{v_{diff,1} - R_{S3}i_g}{(R_{e1} + R_{e2})C_1} \right) - s(t) \left(\frac{I_{PV}}{C_B} + \frac{R_{CB}I_{PV} + v_{diff,2}}{R_{e2} + C_{e2}} \right) \quad (12)$$

where $s(t)$ denotes the switching state function given as follows:

$$s(t) = \begin{cases} 1, & \text{when the circuit is at positive state} \\ 0, & \text{when the circuit is at zero state} \\ -1, & \text{when the circuit is at negative state} \end{cases}$$

The average current of $i_S 1$ and $i_S 3$ during T_s can be found as follows:

$$\langle i_{S1} \rangle_{T2} = \frac{v_{diff,1}T_s + R_{S3}\langle i_g \rangle T_s}{R_{e1} + R_{S3}} \quad (13)$$

$$\langle i_{S3} \rangle_{T2} = \frac{v_{diff,2}T_s + R_{CB}I_{PV}}{R_{e2}} \quad (14)$$

The simulation results of the current flowing through the switches S_1 and S_3 for the output power 500 W are shown in Fig. 7. The value of the current that passes through S_1 and S_3 to reach to its maximum at the negative state is shown in this figure too. At the negative state,

$$\langle i_{S1,max} \rangle_T = \frac{1}{2} \left(\frac{C_1}{C_1 + C_2} + 1 \right) \left(\frac{M I_m}{1 - M} + \frac{T_s}{R_{e1} C_{e1}} \frac{1 - M}{2} \right) \quad (15)$$

$$\langle i_{S3,max} \rangle_T = \frac{1}{2} \left(\frac{C_1}{C_1 + C_B} + 1 \right) \left(\frac{M I_m}{1 - M} + \frac{T_s}{R_{e2} C_{e2}} \frac{1 - M}{2} \right) \quad (16)$$

Equations (22) and (23) indicate that the values of $C_1/(C_1 + C_2)$ and $C_1/(C_1 + C_B)$ should be calculated small enough, and the values of the $R_{e1}C_{e1}$ and $R_{e2}C_{e2}$ should be smaller than the switching period in order to minimize the current stress on the switches.

These values can be limited by a small resistor or a small inductor between the capacitors if needed. The relationship between the voltage and current passing through the capacitors is calculated by

$$i_C = C \frac{\Delta v_C}{\Delta t} \quad (17)$$

The required capacitance of C_1 and C_B for the proposed inverter can be derived by equaling the capacitor power magnitude to the grid power ripple magnitude. The capacitance C_1 and C_B can be calculated as follows:

$$C_1 \text{ or } C_B = \frac{I_{C1} \text{ or } I_{CB}(\max)}{\Delta V_r \Delta V_n f} \quad (18)$$

where I_{C1} and I_{CB} are the maximum current that passes through the capacitors C_1 and C_B , respectively. ΔV_r , ΔV_n , and f are the capacitor voltage

ripple magnitude, nominal voltage on the capacitor, and the frequency during maximum current, respectively.

B.CONDUCTION AND SWITCHING LOSSES OF POWER DEVICES

During the positive power cycle, the grid current flows through switches S_1 and S_2 and the capacitor C_1 is charged through diode D_2 at the positive state as shown in Fig. 6(a) and (g). The capacitor C_1 is charged through diode D_2 and switch S_1 at the negative state as shown in Fig. 6(c) and (e). The voltage drop of the power devices can be derived by

$$\text{MOSFET: } v_{DS}(t) = i(t)R_{DS} \quad (19)$$

$$\text{Diode: } v_{AK}(t) = V_F + i(t)R_{AK} \quad (20)$$

where v_{DS} is the drain source voltage drop of the MOSFET, R_{DS} is the drain source resistance of the MOSFET during on the state operation, v_{AK} is the anode cathode voltage drop of the diode, V_F is the equivalent voltage drop under zero current condition of the diode, R_{AK} is the anode cathode resistance of the diode during the on state, and $i(t)$ is the grid current. The average value of the conduction losses of the MOS FET switch (PMOSFET Cond) during half of the fundamental period is calculated by

TABLE I
Duty Ratio Of Each Conducting Device

Semiconductor devices	duty ratio (d) positive cycle ($v_g > 0$) negative cycle ($v_g < 0$)	
S_1	$M \sin \omega t$	$M \sin \omega t$
S_2	1	$1 - M \sin \omega t$
S_3	$M \sin \omega t$	$1 - M \sin \omega t$
S_4	0	$M \sin \omega t$
D_1	0	$M \sin \omega t$
D_2	$M \sin \omega t$	0

$$P_{MOSFET_Cond} = \frac{1}{\pi} \int_0^\pi v_{DS}(t) i(t) d_{MOSFET}(t) d\omega t \quad (21)$$

The average value of the conduction loss in the diode (PDiode Cond) during the on state mode is calculated by

$$P_{Diode_Cond} = \frac{1}{\pi} \int_0^\pi v_{AK} i(t) d_{Diodes}(t) d\omega t = \frac{1}{\pi} \int_0^\pi v_F i(t) R_{AK} i(t) d_{Diodes}(t) d\omega t \quad (22)$$

The device manufacturer and circuit parameters for efficiency evaluation of proposed inverter are listed in Table II. The switching losses of the MOSFET switch can be found as follows:

TABLE II
Specifications And Power Devices For Efficiency Evaluation

Parameter	Value
Input Voltage	400 V
Grid voltage/frequency	220V/50 HZ

Rated power	500 W
Ac Output Current	2.3A
Switching frequency	24 KHZ
Duty ratio (M)	0.78

$$P_{MOSFET_SW} = f_{SW} E_{OSS} V_F \quad (23)$$

where E_{OSS} is the stored energy that can be achieved from the datasheet that is equal to 45 μJ . The total switching losses of the switches in the proposed inverter can be derived as follows:

$$P_{Total-SW} = 4f_{SW} E_{OSS} V_F = 3.46 W \quad (24)$$

C. Conduction Losses in the Capacitors

The ESR of the capacitors of the proposed inverter is achieved from aluminum electrolyte capacitor datasheets and it is divided into two parts. The second part of the conduction losses is related to the inrush current during the charging of the capacitors. These losses can be defined as follows:

$$P_{CAP_Cond_1} = \frac{2(R_{C1}+R_{CB})}{\pi} \int_0^\pi d_c(t) i_{s1}^2(t) d\omega t \quad (25)$$

$$P_{CAP_Cond_2} = \frac{2(R_{C1}+R_{C2})}{\pi} \int_0^\pi d_c(t) i_{s3}^2(t) d\omega t \quad (26)$$

where $d_c(t)$ is the duty ratio of the capacitor.

D. Control Scheme

The control strategy of the proposed grid-tied single-phase inverter is shown in Fig. 9. It contains two cascaded loops [21]: the first loop is an inner control loop, which has the responsibilities to generate a sinusoidal current and the outer control loop is implemented for the current reference generation, where the power is controlled. The transfer function of this controller can be found as follows:

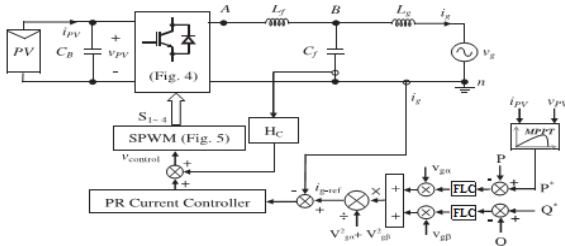


Fig. 9. Control block diagram of the proposed single-phase grid-tie inverter based on single-phase PQ theory.

$$G_{PR(s)} = K_p + \frac{2K_r}{s^2 + \omega^2} \quad (27)$$

where k_p is the proportional gain, k_r is the fundamental resonant gain, and ω is the resonant frequency. According to the single-phase PQ theory the current reference can be produced by regulating the active and reactive powers. The active power (P) and reactive power (Q) for the proposed topology can be calculated by

$$P = \frac{v_{g\alpha} i_{g\alpha} + v_{g\beta} i_{g\beta}}{2}, Q = \frac{v_{g\alpha} i_{g\alpha} - v_{g\beta} i_{g\beta}}{2} \quad (28)$$

where $v_{g\alpha}$, $v_{g\beta}$, $i_{g\alpha}$, and $i_{g\beta}$ are the α and β components of grid voltage and current, respectively. The active power and reactive power references (P^* and Q^*)

can be tuned by the operators $\{R-3\}$ or in the control unit, when the MPPT control is activated. If PI controllers are used for power regulations, the grid current reference (i_{g-ref}) can be derived as follows [24]:

$$i_{g-ref} = \frac{1}{v_{g\alpha}^2 + v_{g\beta}^2} [v_{g\alpha} \ v_{g\beta}] \begin{pmatrix} G_p(s) & (P - P^*) \\ G_q(s) & (Q - Q^*) \end{pmatrix} \quad (29)$$

where $G_p(s)$ and $G_q(s)$ are the PI controllers for active power and reactive power, respectively.

The LCL filter is adopted as the grid interfaced filter in this proposed topology. High output current quality in the proposed inverter can be obtained if the output filter is configured correctly. The inverter-side inductor (L_f) value is calculated by considering 10–20% of the ripple on the output current, which is given by

$$L_f = \frac{(v_{dc} - v_{An})(M \sin \omega t)}{f_{SW} \Delta i_L} \quad (30)$$

where f_{sw} is the switching frequency and Δi_L represents the peak-to-peak ripple current on the L_f . The inverter output voltage (v_{An}) can be calculated as follows:

$$v_{An} = M V_{dc} \sin \omega t \quad (31)$$

By replacing (31) with (30) and simplifying it, we have

$$L_f = \frac{(v_{dc})(RF)}{f_{sw} \Delta i_L} \quad (32)$$

where RF is the ripple current and can be calculated from

$$RF = M \sin \omega t - M^2 \sin^2 \omega t \quad (33)$$

The maximum achievable value of modulation index (M) is $RF_{max} = 0.25$ [26]. The maximum value of the filter capacitor is calculated by (42), limiting to be less than 5% of the nominal value [27]

$$C_{F,max} = \frac{0.05 P_n}{2\pi f V_{rms}^2} \quad (34)$$

where P_n is the nominal power, V_{rms} denotes the root mean square (RMS) grid voltage, and f presents the grid frequency. There is a relation between the inverter-side inductor (L_f) and the grid side (L_g). This value is determined with the ratio between the ripple attenuation (r) as described in [28]

$$L_g = r L_f \quad (35)$$

The grid-side inductor (L_g) value can be determined by

$$10f \leq f_{res} \leq 0.5f_{sw} \quad (36)$$

The resonant frequency for the LCL filter is given by

$$f_{res} = (1/2\pi) \sqrt{(L_f + L_g)/L_f L_g C_f} \quad (37)$$

The active damping is used to smooth the resonance peak of the LCL filter as shown in Fig. 9. A block diagram of the control system is shown in Fig. 10. The Bode diagram of the transfer function from v_{cref} to i_g is defined by $G(s)$. This diagram is shown in Fig. 11 in order to demonstrate the effect of active damping by the filter capacitor current (H_{cic})

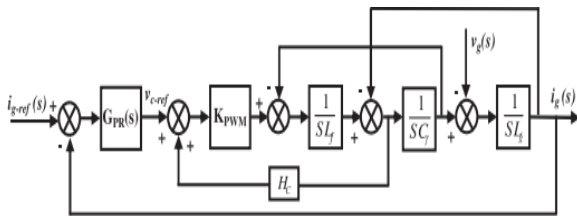


Fig. 10. Control diagram of the injected current with capacitor current feedback active damping.

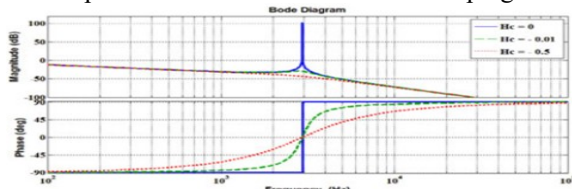


Fig. 11. Bode plot of the system in the case of different values for the active damping gain HC

$$G(s) = \frac{K_{PWM} G_1(s)}{1 + H_c K_{PWM} C_f L_\theta G_1(s)^2} \quad (38)$$

and $K_{pwm} = 1$ and H_c is the active damping gain.

E. Comparison With Other Known Topologies

A comparison of the transformerless inverter structures with respect to number of semiconductor devices, passive elements, THD of the current, and number of switches in the current path is listed in Table III.

TABLE III
comparison of the proposed topology with the conventional transformerless topologies

Converter	Semiconductor devices				Switches in the current path	THDi (%)
	Switches	Diodes	C	L		
H5	5	0	1	3	3	2
HERIC	6	0	1	3	2	1.9
CM in [31]	7	2	2	2	4	2.5
CM in [32]	6	0	3	2	3	2.8
CM in [33]	6	6	2	2	3	2.2
Proposed	4	2	3	2	2	2.1

This comparison includes conventional H5, HERIC inverter, and several common ground transformer less inverters like [31]–[33] with the proposed inverter. It can be seen from Table III that the proposed Thus, these topologies need extra filters to absorb the CM current according to Table III and the analysis given in Section I.

The number of switches in the current path is related to the conduction losses. Fig. 12 shows the power semiconductor losses distribution according to the switching frequency at the rated power of all inverter topologies listed Table III with the same circuit parameters.

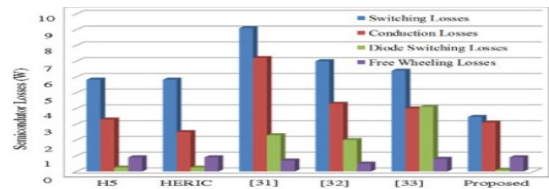


Fig. 12. Total semiconductor power losses distribution for the H5, HERIC, [31]–[33] and the proposed topologies at rated power.

FUZZY LOGIC CONTROLLER

In FLC, basic control action is determined by a set of linguistic rules. These rules are determined by the system. Since the numerical variables are converted into linguistic variables, mathematical modeling of the system is not required in FC.

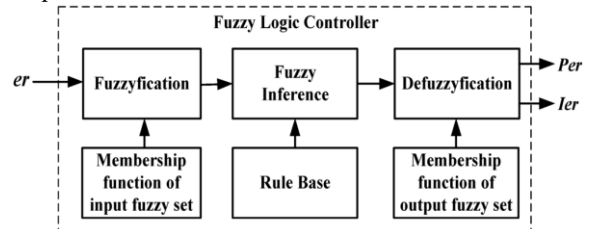


Fig.13.Fuzzy logic controller

The FLC comprises of three parts: fuzzification, interference engine and defuzzification. The FC is characterized as i. seven fuzzy sets for each input and output. ii. Triangular membership functions for simplicity. iii. Fuzzification using continuous universe of discourse. iv. Implication using Mamdani's, 'min' operator. v. Defuzzification using the height method.

TABLE III: Fuzzy Rules

e	NB	NM	NS	ZE	PS	PM	PB
NB	NB	NB	NB	NB	NM	NS	ZE
NM	NB	NB	NB	NM	NS	ZE	PS
NS	NB	NB	NM	NS	ZE	PS	PM
ZE	NB	NM	NS	ZE	PS	PM	PB
PS	NM	NS	ZE	PS	PM	PB	PB
PM	NS	ZE	PS	PM	PB	PB	PB
PB	ZE	PS	PM	PB	PB	PB	PB

Fuzzification: Membership function values are assigned to the linguistic variables, using seven fuzzy subsets: NB (Negative Big), NM (Negative Medium), NS (Negative Small), ZE (Zero), PS (Positive Small), PM (Positive Medium), and PB (Positive Big). The input error for the FLC is given as

$$E(k) = \frac{P_{ph(k)} - P_{ph(k-1)}}{V_{ph(k)} - V_{ph(k-1)}} \quad (39)$$

$$CE(k) = E(k) - E(k-1) \quad (40)$$

Inference Method: Several composition methods such as Max–Min and Max-Dot have been proposed in the literature. In this paper Min method is used. The output membership function of each rule is given by the minimum

operator and maximum operator. Table 1 shows rule base of the FLC.

Defuzzification: As a plant usually requires a non-fuzzy value of control, a defuzzification stage is needed. To compute the output of the FLC, „height“ method is used and the FLC output modifies the control output. Further, the output of FLC controls the switch in the inverter. To achieve this, the membership functions of FC are: error, change in error and output

The set of FC rules are derived from

$$u = -[\alpha E + (1-\alpha) * C] \quad (41)$$

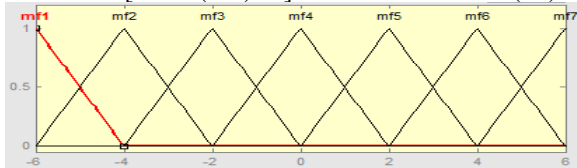


Fig 14 input error as membership functions

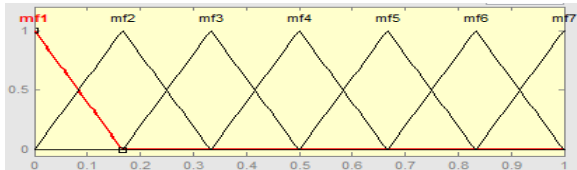


Fig 15 change as error membership functions

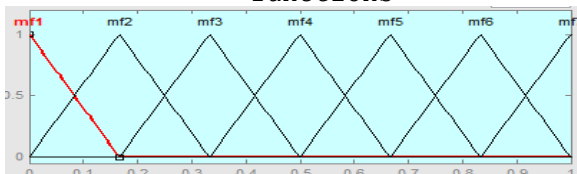


Fig.16 output variable Membership functions

Where α is self-adjustable factor which can regulate the whole operation. E is the error of the system, C is the change in error and u is the control variable.

SIMULATION RESULTS

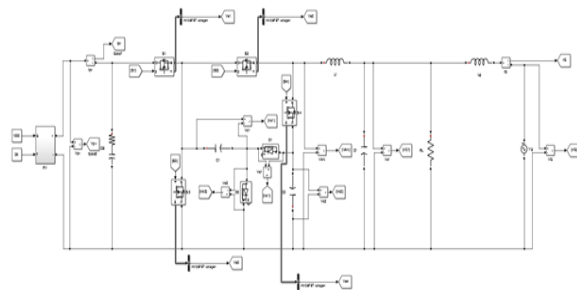


Fig: 17 simulation block diagram of proposed single-phase transformer less grid-connected inverter

In fig 17 the proposed grid connected inverter will operate with the unity power factor (PF = 1) will seen in simulation results.

The simulation results of the proposed grid-connected inverter with unity power factor (PF = 1) operation are presented in Fig18

TABLE IV
Parameters For The 500 W

Parameter	Value	Parameter	Value
Power rating (P)	500 W	Capacitance (C_1)	220 μ F, 500 V
Input voltage (V_{dc})	400V	Capacitance (C_2)	330 μ F, 500 V
Output voltage (V_{Bn})	220 V (RMS)	L filter (L_f)	4 mH
Input capacitor (C_B)	470 μ F, 500 V	C filter (C_f)	2.2 μ F
Power switches ($S_1 - S_4$)	C2M0080120D, SiC MOSFET	L_g	2 mH
Diodes (D_1, D_2)	C3D10060A Schottky Diode	Switching frequency (f_s)	24 kHz

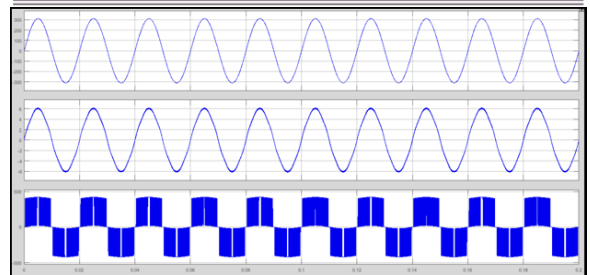


Fig. 18 Simulation results of the proposed topology with unity power factor (PF = 1) operation. (a) v_g [500 V/div], (b) i_g [5 A/div], (c) v_{An} [500 V/div], and (d) fast Fourier transform analysis of i_g [50 V/div and 125 Hz/div].

From Fig. 18, it is clear that the output current and voltage of the proposed inverter are highly sinusoidal with low harmonic distortion due to the three-level inherency of the output voltage. The current harmonic distribution is demonstrated in Fig. 13.

Figs. 19 and 20 demonstrate the simulation results for the inverter operating under current lagging condition (PF = + 0.8) and leading condition (PF = -0.8), respectively.

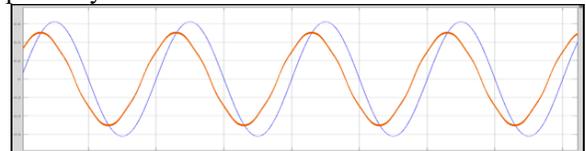


Fig. 19. Simulation results of the proposed topology with lagging power factor operation. (a) v_g [500 V/div] and (b) i_g [2 A/div].

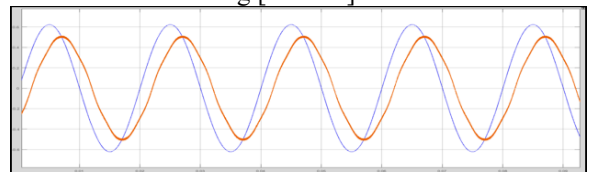


Fig. 20. Simulation results of the proposed topology with leading power factor operation. (a) v_g [500 V/div] and (b) i_g [2 A/div].

The partial enlargement of the grid current i_g , grid voltage v_g , and three level output voltage v_{An} is provided in Fig. 21. It is clear that the pulse duration of the output voltage (v_{An}) is in agreement with the switching

frequency. The voltage stress of the capacitors and diodes is shown in Fig. 22.

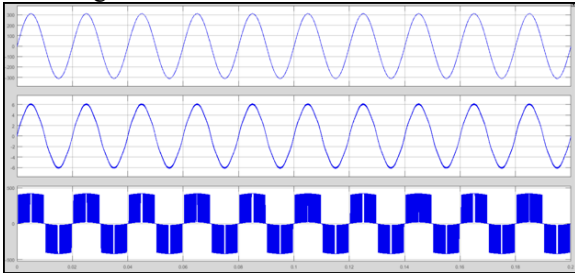


Fig. 21. Simulation enlarged results of the proposed topology. (a) v_{An} [500 V/div], (b) v_g [250 V/div], and (c) i_g [5 A/div], time [400 μ s/div]

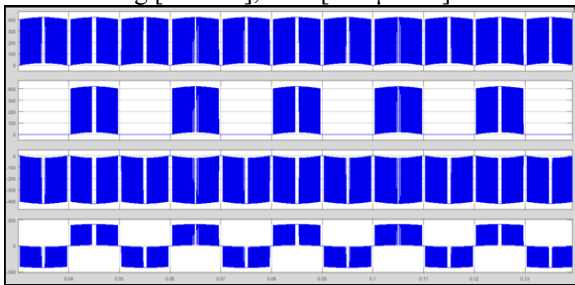


Fig. 22. Simulation results for drain source voltage of switches. (a) v_{S1} [250 V/div], (b) v_{S2} [500 V/div], (c) v_{S3} [250 V/div], and (d) v_{S4} [500 V/div].

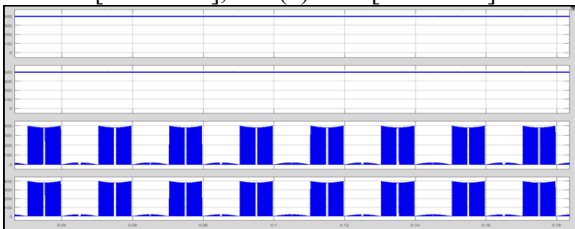


Fig. 23. Simulation results of the capacitor and diode voltages. (a) v_{C1} [250 V/div], (b) v_{C2} [500 V/div], (c) v_{D1} [250 V/div], and (d) v_{D2} [250 V/div].

Fig. 23 (a)–(c) shows the simulation waveforms of the grid voltage v_g , the grid current i_g , and the CM voltage v_{CM} in the proposed topology.

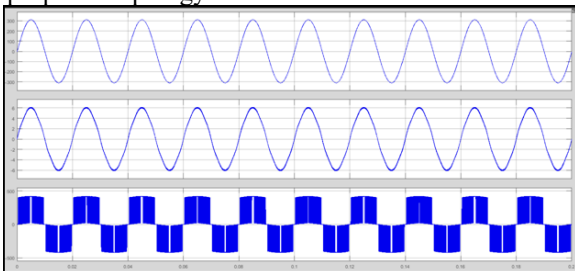


Fig. 24. Simulation results of the proposed topology. (a) v_g [250 V/div], (b) i_g [5 A/div], and (c) v_{CM} [200 V/div].

The performance of the control strategy is confirmed by applying a step change to the proposed inverter. A PR current controller is adopted with $k_i = 2000$

and $k_p = 20$ as shown in (35). Fig. 25 shows the performance of the proposed inverter under the load step change. From fig :26 total harmonics distortion of the proposed topology .

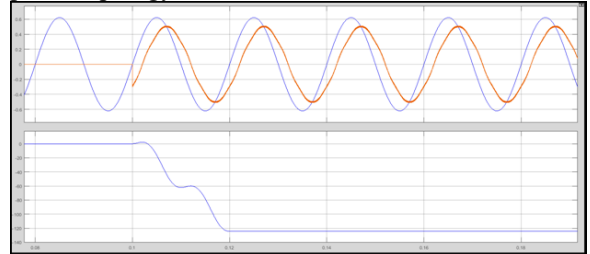


Fig. 25. Simulation results of the proposed topology in dynamic state. (a) v_g [250 V/div], (b) i_g [10 A/div], and (c) active power (P) [400 W/div].

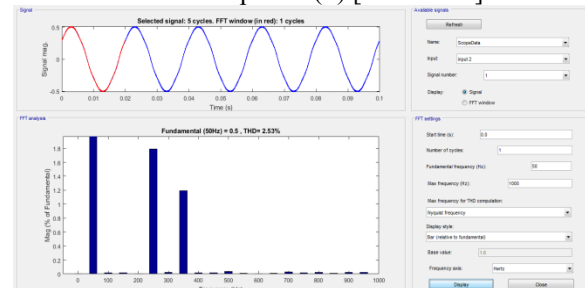


Fig : 26 total harmonics distortion
CONCLUSION

In this paper we are implementing a new single-phase transformer less inverter for a grid-tied PV system using a charge pump circuit concept with the fuzzy controller. Therefore the main concept of the proposed system is to generate the negative output voltages which have been developed in this proposed inverter. Here we are using the fuzzy logic controller for the better performance because the fuzzy controller is the most suitable for the human decision-making mechanism, providing the operation of an electronic system with decisions of experts. Therefore we are developing the proposed topology which is similar to the neutral line in the grid; therefore the leakage current will be suppressed and the transformer is eliminated. Moreover the proposed topologies have the capability to deliver the required reactive power into the grid. Therefore the proposed topology is used to realize the minimum number of components and higher power density can be achieved with lower design cost. By using the simulation result we can verify the proposed system.

REFERENCES

- [1] S. B. Kjaer, J. K. Pedersen, and F. Blaabjerg, "A review of single-phase grid connected inverters for photovoltaic modules," *IEEE Trans. Ind. Electron.*, vol. 41, no. 5, pp. 1292–1306, Sep./Oct. 2005.
- [2] X. Guo, R. He, J. Jian, Z. Lu, X. Sun, and J. M. Guerrero, "Leakage current elimination of four-leg inverter

- for transformerless three-phase PV systems,” IEEE Trans. Power Electron., vol. 31, no. 3, pp. 1841–1846, Mar. 2016.
- [3] W.-J. Cha, K.-T. Kim, Y.-W. Cho, S.-H. Lee, and B.-H. Kwon, “Evaluation and analysis of transformerless photovoltaic inverter topology for efficiency improvement and reduction of leakage current,” IET Power Electron., vol. 8, no. 2, pp. 255–267, 2015.
- [4] H. Xiao and S. Xie, “Leakage current analytical model and application in single-phase transformerless photovoltaic grid-connected inverter,” IEEE Trans. Electromagn. Compat., vol. 52, no. 4, pp. 902–913, Nov. 2010.
- [5] T. Bruckner, S. Bernet, and H. G ¨uldner, “The active NPC converter and its loss-balancing control,” IEEE Trans. Ind. Electron., vol. 52, no. 3, pp. 855–868, Jun. 2005.
- [6] D. Barater, E. Lorenzani, C. Concari, G. Franceschini, and G. Buticchi, “Recent advances in single-phase transformerless photovoltaic inverters,” IET Renewable Power Gener., vol. 10, no. 2, pp. 260–273, 2016.
- [7] W. Yu et al., “High-efficiency inverter with H6-type configuration for photovoltaic non-isolated ac module applications,” in Proc. Annu. IEEE Appl. Power Electron. Conf. Expo., 2010, pp. 1056–1061.
- [8] B. Yang, W. Li, Y. Gu, W. Cui, and X. He, “Improved transformerless inverter with common-mode leakage current elimination for a photovoltaic grid connected power system,” IEEE Trans. Power Electron., vol. 27, no. 2, pp. 752–762, Feb. 2012.
- [9] F. Bradaschia, M. C. Cavalcanti, P. E. P. Ferraz, F. A. S. Neves, E. C. Santos, and J. H. G. M. da Silva, “Modulation for three-phase transformerless z-source inverter to reduce leakage currents in photovoltaic systems,” IEEE Trans. Ind. Electron., vol. 58, no. 12, pp. 5385–5395, Dec. 2011.
- [10] Y. Gu, W. Li, Y. Zhao, B. Yang, C. Li, and X. He, “Transformerless inverter with virtual dc bus concept for cost-effective grid-connected PV power systems,” IEEE Trans. Power Electron., vol. 28, no. 2, pp. 793–805, Feb. 2013.